Table 1 Patients' characteristics

No.	Age (m)/gender	Tumor size (cm)	AFP (ng/mL)	Tumor site	Obstruction or stenosis of PV or IVC	AST/ALT (IU/L)	PRETEXT	Histology
1	15/F	15	1,839,700	MAP	RPV	196/75	III	Well differentiated
2	18/M	13	634,000	AP	IVC	27/10	II	Poorly differentiated
3	22/M	11	267,000	MAP	RPV	40/12	III	Poorly differentiated
4	11/M	6	26,895	MAP	Patent	47/13	III	Poorly differentiated
5	4/M	8.5	158,773	LMA	Main PV	35/14	III	Poorly differentiated
6	38/M	11	30,416	MAP	Patent	23/5	III	Poorly differentiated
7	3/F	16	954,300	LMAP	PV	113/15	IV	Poorly differentiated
8	10/F	14	484,000	LMA	LPV	96/35	III	Poorly differentiated
Mean	15.2	11.8	549,386			72/22	–	–

Tumor site: *L* lateral segment, *M* medial segment, *A* anterior segment, *P* posterior segment

Tumor size Max diameter of tumor, *AFP* alfa-fetoprotein, *PV* portal vein, *RPV* right portal vein, *LPV* left portal vein, *IVC* inferior vena cava, *AST* aspartate aminotransferase, *ALT* alanine aminotransferase

Then, 2–5 mL iodized oil (Lipiodol; Laboratoire Guerbet, Roissy Charles de Gaulle, France), a contrast material containing 1/3 iodized oil, and 30 mg/m^2 THP-ADR were mixed by pumping 10 times by use of a three-way stopcock valve and two 5–10-mL syringes. The dosage of lipiodol was adjusted individually depending on tumor size, necrotic area assessed by enhanced CT, hepatic angiographic findings, and the clinical status of each patient. THP-ADR dispersed in lipiodol was injected into the feeding artery of the tumor until near-complete stasis of the feeding artery had occurred on angiography. The TACE procedure was performed once only. In this study, hepatoblastomas were not embolized with gelatin sponge particles.

Subsequent surgical resection was usually performed ~3 weeks after TACE, when the tumor volume appeared to have decreased sufficiently to enable safe resection by either lobectomy or extended lobectomy. In five cases, two courses of postoperative systemic chemotherapy were added. The chemotherapy regimen consisted of repeated courses of CDDP, 80 mg/m^2 × 1 day, and THP-ADR, 30 mg/m^2 × 2 days or IFO, 3.0 mg/m^2/day × 2, or THP-ADR, 30 mg/m^2/day × 2, etoposide (VP16),100 mg/m^2/day × 5, and carboplatin, 400 mg/m^2/day.

Assessment

The effects of preoperative systemic chemotherapy and TACE were evaluated on the basis of AFP level and tumor volume, calculated by use of the equation volume = 1/2 × length × (transverse diameter)^2, with follow-up CT. In addition, tumor response after systemic chemotherapy and TACE was classified into four grades in accordance with the modified Response Evaluation Criteria for Solid Tumors (mRECIST). The extent of tumor necrosis was histologically evaluated as the percentage necrotic or fibrotic area in the largest section of the surgical specimen. Adverse events related to the TACE were evaluated on the basis of the Common Terminology Criteria for Adverse Events ver. 3.0 and the SIR complication classification system. Tumor recurrence and survival were assessed by reviewing medical records and follow-up enhanced CT. Medical check and monitoring of AFP were conducted 3-monthly; enhanced CT was conducted within 1 month postoperatively, at 3 months, and then every 6 months for 2 years. After the 2nd year, enhanced CT was alternated on a 6-month basis. The follow-up periods after treatment ranged between 13 and 93 months (mean 59 months).

Results

The results of preoperative systemic chemotherapy and TACE are summarized in Table 2.

The number of preoperative systemic chemotherapy cycles ranged from 4 to 6, with a mean of 4.5. The time interval between preoperative systemic chemotherapy and TACE ranged from 16 to 37 days, with a mean value of 26.8 days. The dosage of lipiodol ranged from 2 to 5 (mean 3.9) mL.

Response to preoperative systemic chemotherapy and TACE was as follows. A marked reduction in tumor size associated with a decrease in AFP level occurred after preoperative systemic chemotherapy and TACE (Table 3). After preoperative systemic chemotherapy, compared with initial levels, mean tumor shrinkage was 44.3 % (0–71.9 %) and mean AFP decrease was 63.4 % (0–99.8 %). For all children with obstruction of the portal vein and IVC before treatment, these obstructions were improved after preoperative systemic chemotherapy. After

Table 2 Results of preoperative systemic chemotherapy and TACE

No.	CITA (kur)	Tumor size after CITA (cm)	Time interval from CITA (day)	Catheter system (Fr)	Carboplatin (mg)	ADR (mg)/ LPD (mL)	Treated vessels: infused drug ratio	Procedure time (min)
1	4	11	37	4	80	12/5	RHA: 4 LHA: 1	68
2	5	8.7	28	4	80	13/5	RHA	55
3	4	7.8	23	4	90	11/4.8	RHA	60
4	4	4.5	16	4	90	13/2	A4: 2 RHA: 1	50
5	5	9.6	28	3	60	9/3.6	PHA	55
6	4	10	28	3	100	16/5	RHA: 9 A3: 1	60
7	6	8.5	20	3	50	7.4/2.5	MHA: 9 RHA: 1	100
8	4	7.7	34	3	85	12/3	LHA: 2 MHA: 1	60
Mean	4.5	8.5	26.8	–	79.3	11.6/3.9	–	63.5

CITA preoperative systemic chemotherapy, *cisplatin* 80 mg/m^2/day, *THP-ADR* tetrahydropyranyl-adriamycin 30 mg/m^2/day × 2
CDDP carboplatin, *ADR* tetrahydropyranyl-adriamycin, *LPD* lipiodol

Table 3 Response to preoperative chemotherapy

Patient no.	Tumor shrinkage (%)		AFP decrease (%)		mRECIST		PRETEXT after CITA and TACE	Tumor necrosis (%)
	CITA	CITA + TACE	CITA	CITA + TACE	CITA	CITA + TACE		
1	32.1	51.5	23.0	99.9	PR	CR	II	99
2	52.1	69.3	86.3	97.1	PR	PR	II	80
3	38.1	50.4	81.2	90.1	PR	PR	II	70
4	71.9	81.8	88.8	98.1	PR	CR	I	90
5	0	33.3	0	82.4	PD	PR	II	15
6	21.1	46.4	31.7	93.3	PR	PR	II	85
7	67.9	78.4	97.1	97.6	PR	PR	III	80
8	70.9	76.6	99.8	99.9	PR	PR	II	85
Mean	44.3	60.9	63.4	94.8				75.5

Tumor necrosis: the extent of tumor necrosis was histologically evaluated as percentage necrotic or fibrotic area in the largest section of the surgical specimen

preoperative systemic chemotherapy followed by TACE, compared with initial levels, mean tumor shrinkage was 60.9 % (33.3–81.8 %) and the mean AFP decrease was 94.8 % (82.4–99.9 %). According to modified RECIST criteria, evaluated by enhanced CT, 25 % (2/8) of children achieved complete response and 75 % (6/8) partial response after preoperative systemic chemotherapy followed by TACE. No delay of surgery was encountered. Subsequently, tumor extirpation was performed for all cases (Fig. 1; Table 4), and the time interval between TACE and surgical resection ranged from 19 to 25 days, with a mean of 22 days. Preoperative systemic chemotherapy followed by TACE enabled subsequent safe and complete surgical resection in all cases.

Pathological examination revealed massive necrosis in the excised specimens, and the percentage necrotic area within the tumor ranged from 15 to 99 %, mean 75.5 %. On microscopic examination, all resected specimens had free margins.

Complications and toxicity after TACE

For one child, extravasation of contrast from the superior adrenal artery was recognized during TACE, but it was controlled spontaneously. This complication was classified as A of the Society of Interventional Radiology (SIR) Classification System for Complications by Outcome. There was no femoral puncture complication.

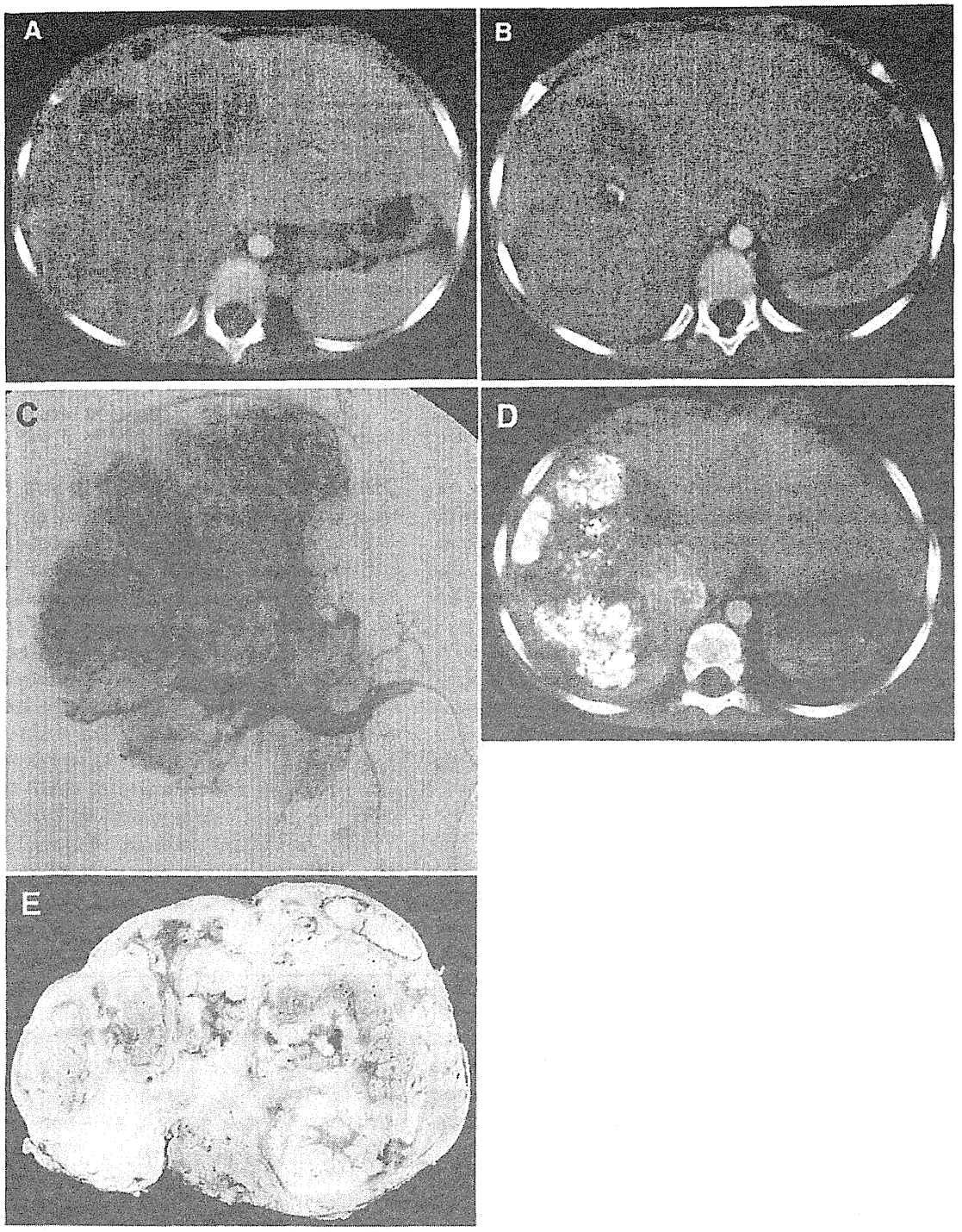

Fig. 1 38-month-old boy with poorly differentiated hepatoblastoma (case 6). Tumor size 11 × 6.4 cm, AFP 30,416 (ng/mL), PRETEXT II. **a** Enhanced CT before treatment reveals a large tumor involving almost the entire right lobe and S4. **b** Enhanced CT after CITA 4 kur. Tumor volume decreased by 21.2 %. **c** Pre-chemoembolization angiogram via the hepatic artery shows a large hypervascular lesion with abundant neovascularity. **d** After TACE, abundant lipiodol deposits appeared in the right lobe and the tumor volume decreased by 32.1 %. **e** Pathological examination of excised specimens showed the percentage necrotic area within the tumor was 85 %. Tumor shrinkage and AFP decrease were, respectively, 21.2 and 31.7 % after 4 kur CITA and 46.4 and 93.3 % after TACE combined with CITA

Table 4 Clinical courses after TACE

No.	Time between surgery and TACE (day)	Operation	Post-operative CTx (kur)	Follow-up (months)	Recurrence	Outcome
1	23	Rt. lobectomy	0	84	–	Alive
2	22	S5 + 6 segmentectomy	0	92	–	Alive
3	22	Rt. lobectomy	2	93	–	Alive
4	23	Tumor resection	0	82	–	Alive
5	25	Rt. lobectomy	2	29	–	Died[a]
6	21	Rt. lobectomy	2	64	–	Alive
7	19	S3, 4, 5, 8 segmentectomy	2	13	Intrahepatic recurrence	Died[b]
8	21	Extended Lt. lobectomy	2	16	–	Alive
	Mean: 22			Mean: 59	12.5 %	75 %

Rt. right, *Lt.* left, *CTx* systemic chemotherapy

[a] Died of a second malignancy (AML)

[b] Died after liver transplantation for intrahepatic recurrence

Grade 1 elevation of fever after TACE was observed for 62.5 % (5/8) of the children. Grade 1 abdominal pain after TACE was observed for 50 % (4/8) of the children. Grade 1 elevation of aspartate aminotransferase (AST) and alanine aminotransferase (ALT) after TACE was observed for 75 % of children (6/8), but no patient suffered from prolonged and severe liver dysfunction. Renal dysfunction, symptoms of myelosuppression, or signs of cardiotoxicity after TACE were not observed for any patient. No patient suffered from TACE-related major complications. No liver failure was noted after surgery and postoperative systemic chemotherapy.

Outcomes

For one patient only, liver metastases were identified in the remaining liver, 2 months after surgery. This patient died of sepsis 4 days after liver transplantation for liver metastases. Recurrence of hepatoblastoma in another patient was not recognized; however, he died of a second malignancy (acute myelogenic leukemia) 23 months after surgery. The other six patients were doing well and were free from disease at last follow-up. During the mean 59-month follow-up, tumor recurrence was 12.5 % and tumor-free survival was 75 %.

Discussion

It has been generally accepted that complete surgical removal of hepatoblastoma is essential for long-term survival [11, 16]. For most patients, however, hepatoblastoma is unresectable at presentation, so several preoperative chemotherapy, including systemic chemotherapy, or TACE protocols are currently used in different centers to increase resectability and improve long-term survival [17, 18]. For patients with unresectable or metastatic hepatoblastoma, the Pediatric Oncology Group (POG) recommended treatment strategy based on intensification of preoperative chemotherapy, depending on tumor response [19]. Recently, response to a variety of chemotherapy protocols, including CDDP and doxorubicin (DOX), has been reported to be 70–76 % [8, 20]. In our series, some patients had a marked response to preoperative systemic chemotherapy with CDDP and THP-ADR—a nearly linear decrease in AFP levels and a reduction in tumor size. For some children, however, poor response to systemic chemotherapy was recognized and reduction of tumor size was insufficient to perform complete surgical resection. Drug resistance is one of the problems of systemic chemotherapy [12]. TACE takes good advantage of the combined antitumor effects of regional chemotherapy and the tumor ischemia caused by occlusion of the feeding artery to achieve maximum reduction in tumor size. TACE can maximize drug uptake by the tumor and minimize exposure of children to drugs [12, 18]. In this study, TACE was performed after it was judged that further tumor shrinkage could not be achieved by additional systemic chemotherapy. For these poor responders to systemic chemotherapy, also, decrease in AFP levels and a reduction in tumor size was observed after TACE. To achieve sufficient tumor reduction to enable its complete resection, TACE seems to have been useful especially for poor responders to systemic chemotherapy. In this study, embolization with gelatin sponges or coils was not conducted to avoid the hepatic infarction or abscess formation related to TACE. Many previous studies on use of TACE for hepatoblastoma reported that TACE using a gelatin sponge was necessary and acceptable. In our many cases, obstruction or stenosis of the portal vein and/or IVC were recognized before treatment. After systemic chemotherapy, partial improvement of major portal vein and/or IVC obstruction was

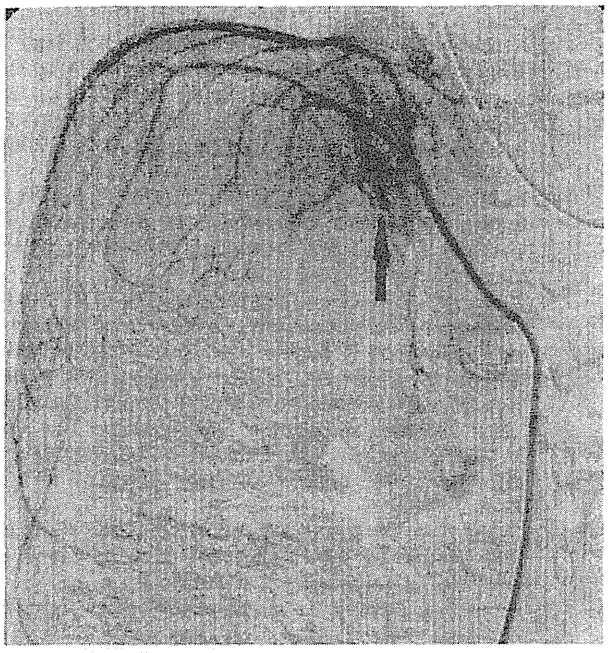

Fig. 2 15-month-old girl with well differentiated hepatoblastoma (case 1). Tumor size 15 cm, AFP 1,839,700 (ng/mL), PRETEXT III. Right inferior phrenic angiogram reveals extravasation of contrast from superior adrenal artery during TACE (*arrow*); it was controlled spontaneously, however

achieved but obstruction of the second or third portal branches occasionally persisted. Therefore, TACE without a gelatin sponge was used in this study [10–12, 17, 18]. Despite this, however, sufficient tumor shrinkage (mean 60.9 %) and AFP decrease (mean 94.8 %) were achieved to enable complete surgical resection after preoperative systemic chemotherapy followed by TACE. Mean tumor shrinkage in this series compares favorably to other reports of systemic chemotherapy alone or repeated TACE alone [18, 21], but the mean AFP decrease in this study was slightly better than in reports for repeated TACE alone [18]. In this study, TACE combined with systemic chemotherapy also enabled subsequent safe and complete surgical resection for all patients, and all resected specimens had free margins on microscopic examination. The histomorphology of hepatoblastoma also determines the response to treatment, thereby affecting outcome [27]. Though the poorly differentiated subtype was present in seven of the eight patients, pathological examination revealed moderate tumor necrosis (mean 75.5 %). In one child (case 5), tumor necrosis was fair compared with the other children. In almost all previous studies reporting TACE for hepatoblastoma, use of embolic agents resulted in surgical resectability with a low incidence of severe complications [5–8, 12, 18]. Because poor responders to TACE without use of an embolic agent are sometimes recognized, embolic agent might be necessary.

In this study, there were no severe complications after TACE. One reason might be that patency of the portal vein was achieved after preoperative systemic chemotherapy. Major portal vein obstruction is known to be a risk factor for liver infarction after TACE [24]. However, major complications related to use of chemoembolic agents, for example acute liver failure, liver infarction, liver abscess, tumor rupture, or pulmonary embolism, must be considered [22–26]. For one patient, iatrogenic dissection or perforation of the superior adrenal artery was recognized during TACE (Fig. 2), but extravasation of contrast from the superior adrenal artery could not be recognized without embolization on selective angiography after TACE. The risk of complications related to the manipulation of a catheter or guidewire, for example iatrogenic dissection or perforation of the celiac artery and its branches, could be higher for children than for adults because of the smaller diameter of each vessel. Needless to say, skillful and careful handling of the smaller devices under fluoroscopic control is the only way to avoid this risk.

Tumor-free survival (75 %) in this series compares favorably with other reports [12, 19]. The reasons might be that our children had no distant metastasis and our combination of systemic chemotherapy and TACE might be able to control not only the main tumor but also nonvisualized micrometastasis. For one patient, only, with PRETEXT IV (case 7), however, although the tumor responded well to preoperative chemotherapy, and complete surgical resection was performed successfully, the tumor recurred locally 2 months after surgical resection. This may be because preexisting micrometastasis was not controlled by our combined therapy. We agree that liver transplantation offers a chance of curing even patients with PRETEXT IV [28]. In one other patient (case 5), no recurrence was seen during follow-up, but he died 29 months postoperatively as a consequence of secondary malignancy. Although rare, we have to recognize that a second malignancy induced by the extremely high dosage of anticancer drugs is a major problem [14].

One limitation of this study is that the long-term effect of preoperative TACE combined with systemic chemotherapy on fertility or perinatal outcome is unclear and must be further evaluated by use of randomized, controlled trials.

In conclusion, the results of this study suggest that preoperative TACE combined with systemic chemotherapy is effective in inducing surgical resectability of unresectable hepatoblastomas, with a low incidence of complications. These results are encouraging, but we cannot draw firm conclusions because of the small number of patients studied.

Conflict of interest We have no direct or indirect financial interest in the products under investigation or the subject matter discussed in this manuscript.

References

1. Derek J. Perilongo RG hepatoblastoma: an oncological review. Pediatr Radiol. 2006;36(183–186):2.
2. Czauderna P, Otte JB, Roebuck DJ, et al. Surgical treatment of hepatoblastoma in children. Pediatr Radiol. 2006;36:187–91.
3. Brown J, Perilongo G, Shafford E, et al. Pretreatment prognostic factors for children with hepatoblastoma. Results from the International Society of Paediatric Oncology (SIOP) Study SIOPEL 1. Eur J Cancer. 2000;36:1418–25.
4. Hata Y. The clinical features and prognosis of hepatoblastoma: follow-up studies done on pediatric tumors enrolled in the Japanese Pediatric Tumor Registry between 1971 and 1980. Part I. Jpn J Surg. 1990;20:498–502.
5. Nakagawa N, Cornelius AS, Kao SCS, Nakajima Y, Nakada K. Transcatheter oily chemoembolization for unresectable malignant liver tumors in children. J Vasc Interv Radiol. 1993;4:353–8.
6. Oue T, Fukuzawa M, Kusafuka T, Kohmoto Y, Okada A, Imura K. Transcatheter arterial chemoembolization in the treatment of hepatoblastoma. J Pediatr Surg. 1998;33(1771–5):5.
7. Arcement CM, Towbin RB, Meza MP, et al. Intrahepatic chemoembolization in unresectable pediatric liver malignancies. Pediatr Radiol. 2000;30:779–85.
8. Malogolowkin MH, Stanly P, Steele DA, Ortega JA. Feasibility and toxicity of chemoembolization for children with liver tumors. J Clin Oncol. 2000;18:1279–84.
9. Geiger JD. Surgery for hepatoblastoma in children. Curr Opin Pediatr. 1996;8:276–82.
10. Inoue S, Nagao T, Ishida Y, et al. Successful resection of a large hepatoblastoma in a young adult: report of a case. Surg Today. 1995;25:974–7.
11. Tashjian DB, Moriarty KP, Courtney RA, et al. Preoperative chemoembolization for unresectable hepatoblastoma. Pediatr Surg Int. 2002;18(187–189):5.
12. Ohtsuka Y, Matsunaga T, Yoshida H, Kouchi K, Ohnuma N. Optimal strategy of preoperative transcatheter arterial chemoembolization for hepatoblastoma. Surg Today. 2004;34(2):127–33.
13. Farhi DC, Odell CA, Shurin SB. Myelodysplastic syndrome and acute myeloid leukemia after treatment for solid tumors of childhood. Am J Clin Pathol. 1993;100(270–275):8.
14. Moppet J, Oakhill A, Duncan AW. Second malignancies in children: the usual suspects? Eur J Radiol. 2001;38:325–48.
15. Hishiki T, Mtasunaga T, Sasaki F, et al. Outcome of hepatoblastomas treated using the Japanese Study Group for Pediatric Liver Tumor (JPLT) protocol-2: report from JPLT. Pediatr Surg Int. 2010;27:1–8.
16. Schnater JM, Aronson DC, Plaschkes J, et al. Surgical view of the treatment of patients with hepatoblastoma: results from the first prospective trial of the International Society of Pediatric Oncology Liver Tumor Study Group. Cancer. 2002;94:1111–20.
17. Ehrlich PF, Greenberg ML, Filler RM. J Improved long-term survival with preoperative chemotherapy for hepatoblastoma. Pediatr Surg. 1997;32(7):999–1002.
18. Li JP, Chu JP, Yang JY, Chen W, Wang Y, Huang YH. Preoperative transcatheter selective arterial chemoembolization in treatment of unresectable hepatoblastoma in infants and children. Cardiovasc Interv Radiol. 2008;31(6):1117–23.
19. Katzenstein HM, Londo WB, Douglass EC, et al. Treatment of unresectable and metastatic hepatoblastoma: a Pediatric Oncology Group Phase II study. J Clin Oncol. 2002;20:3438–44.
20. Ortega JA, Douglass EC, Feusner JH, et al. Randomized comparison of cisplatin/vincristine/fluorouracil and cisplatin/continuous infusion doxorubicin for treatment of pediatric hepatoblastoma: a report from the Children's Cancer Study Group and the pediatric Oncology Group. J Clin Oncol. 2000;18:2665–75.
21. Bajpai M, Pal K, Agarwala S, Seth T, Gupta AK. Midterm results with hepatectomy after preoperative chemotherapy in hepatoblastoma. Pediatr Surg Int. 2005;21:364–8.
22. Chung JW, Park JH, Im JG, Han JK, Han MC. Pulmonary oil embolism after transcatheter oily chemoembolization of hepatocellular carcinoma. Radiology. 1993;187:689–93.
23. Yamaura K, Higashi M, Akiyoshi K, Itonaga Y, Inoue H, Takahashi S. Pulmonary lipiodol embolism during transcatheter arterial chemoembolization for hepatoblastoma under general anaesthesia. Eur J Anaesth. 2000;17:704–8.
24. Sakamoto I, Aso N, Nagaoki K, et al. Complications associated with transcatheter arterial embolization for hepatic tumors. Radiographics. 1998;18:605–19.
25. Hanazaki K, Kajikawa S, Horigome N, et al. Gas-forming liver abscess after transcatheter arterial embolization for hepatocellular carcinoma: report of a case. Surg Today. 1993;23(747–9):28.
26. Tarazov PG. Iodized oil in the portal vein after arterial chemoembolization of liver metastases—a caution regarding hepatic necrosis. Acta Radiol. 1994;35:143–6.
27. Brown BF, Drehener DM, Saldivar VA. Hepatoblastoma a rare pediatric neoplasm. Mil Med. 1993;58:51–5.
28. Otte JB, Pritchard J, Aronson DC, et al. Liver transplantation for hepatoblastoma: results from the International Society of Pediatric Oncology (SIOP) study SIOPEL-1 and review of the world experience. Pediatr Blood Cancer. 2004;42:74–83.

第7章　各疾患における遺伝子治療、遺伝子診断の現状と

今後有望な開発ターゲットの考察

第11節　小児固形悪性腫瘍における遺伝子解析による悪性度診断と遺伝子治療

京都府立医科大学　小児外科　教授　医学博士

田尻　達郎

(株)技術情報協会
書籍「遺伝子治療・診断の最先端技術と新しい医薬品・診断薬の開発」
(2014.5.30 発刊)抜刷

第 11 節　小児固形悪性腫瘍における遺伝子解析による悪性度診断と遺伝子治療

はじめに

小児固形悪性腫瘍は症例毎にその腫瘍の悪性度が様々であることから，その治療にあたっては，まず腫瘍の悪性度を判定することが必要不可欠である。主に分子生物学的手法を使ったトランスレーショナルリサーチを実際に治療を行う臨床医自身が携わることは，症例毎の高度なテーラーメイド型治療につながる。本稿においては，これまで行ってきた神経芽腫を中心とした悪性度を判定する予後関連遺伝子解析の内容を紹介し，また，難治性小児固形悪性腫瘍に対する新規治療法として樹状細胞を用いた免疫遺伝子治療の開発を併せて紹介する。

1.　神経芽腫予後関連遺伝子の数的変化の高感度遺伝子解析

神経芽腫は脳腫瘍以外の小児固形悪性腫瘍で最も頻度が高く，神経堤由来の細胞が腫瘍化したもので副腎髄質，交感神経幹に多く発生する。神経芽腫の生物学的特性は多岐にわたり，悪性度の程度に合わせた至適治療を行うため，分子生物学的手法を用いて予後と関連した遺伝学的異常を迅速かつ正確に同定することが重要である。

神経芽腫の臨床的予後因子としては，年齢（1 才未満は予後良好），臨床病期，原発部位（副腎原発は，その他の部位に比較して予後不良），組織分類（Shimada 分類）などがあげられる。生物学的予後因子には，MYCN 遺伝子増幅，DNA ploidy，1p LOH，11q LOH，17q gain などがあげられるが，その中でも最も強力な予後関連遺伝子として，その数的変化の測定が悪性度判定に必要不可欠であったものが MYCN 遺伝子の増幅である[1]。MYCN 増幅症例の予後は非常に悪いことから，1991 年以降，日本の進行神経芽腫のスタディグループでは MYCN 増幅の有無（MYCN 増幅が 10 コピー以上か否か）に基づいて 2 つの化学療法のレジメが用いられてきた[2]。そのため，MYCN 増幅の状況を迅速かつ正確に判定することが治療上求められる。その解析法は，従来，サザンブロット法による解析が一般的であり，10 コピーを境界として悪性度の判定を行っていた。ただ，これは腫瘍組織全体の解析法であり，腫瘍内の heterogeneity は評価できない。一方，FISH 法（fluorescence in situ hybridization）は個々の神経芽腫細胞の MYCN 増幅の状況を評価できるが定量性に欠く。また，定量的 PCR は，FISH 法のように個々の細胞における評価はできないが，組織全体における遺伝子数量の測定に関しては，サザンブロット法より簡便に短時間で施行可能で感度が高い手法である[3]。我々は，以前より FISH 法のように in situ で個々の細胞を検索できる手法を併用することにより，腫瘍組織内における MYCN 増幅細胞を高感度に把握することができることを報告してきたが[4]，神経芽腫における定量的 PCR 法による MYCN 増幅解析の臨床的意義を確定させるために，さらに多数の神経芽腫検体において本法による解析を行い，サザンブロット法，及び FISH 法による解析結果と比較検討した。

その結果，サザンブロットにて MYCN が single copy であった 54 例中内 46 例は MYCN gene dosage（MYCN / p53）は 2.0 未満だった。2.0 以上を示したのは 8 例ですべて stage 3,4 症例，そのうち 3 例は腫瘍死している。また，サザンブロットで MYCN が 2 コピー以上の 12 例において定量的 PCR での MYCN gene dosage の値は全て 10.0 以上で，そのほとんどが，サザンブロットの値より高値を示した。サザンブロットにて single copy であった症例で，FISH を用いて MYCN 増幅を検索できた 23 例の MYCN gene dosage を clinical stage 別に見ると，非進行症例（stage 1,2,4S）は 18 例，進行症例（stage 3,4）は 5 例で，gene dosage が 2.0 以上を示したものは進行症例の 2 例のみで，その 2 例だけが FISH にて MYCN 増幅細胞を検体中に認めた。症例 1 は，検体中の有核細胞の 15%，症例 2 は 29%にそれぞれ MYCN 増幅細胞を認め，腫瘍内の heterogeneity が疑われた（図 1）。これらの結果から，MYCN 増幅解析は，定量的 PCR と FISH 法の組み合わせが最も高感度であり，治療方針の選択に最も有用であると考えられた[5-7]。現在，国際的にもこの組み合わせによる MYCN 増幅の判定法が標準的とされている。

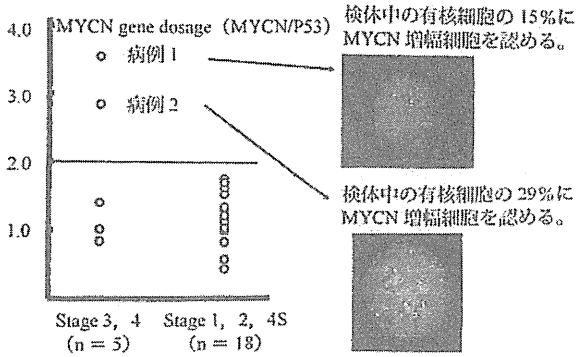

図 1　定量的 PCR と FISH 法による MYCN 遺伝子増幅（サザンブロット MYCN 1 copy 症例）
※カラーの図は巻頭ページを参照

2.　神経芽腫新規予後関連遺伝子の発現量変化による検討

発現量が神経芽腫の予後に関与する遺伝子としては，神経成長因子受容体ファミリーの TrkA（Tropomyosin-Related Kinase A）遺伝子が最も知られているが，我々は新規予後関連遺伝子の検討として，c-MYC 蛋白に結合してアポトーシスを誘導する蛋白として同定されていた BIN1(Bridging integrator 1) 遺伝子の神経芽腫における役割に注目した。BIN1 は神経組織において高発現しており，c-MYC の BIN1 結合部位（MB1）は，MYCN と 100%のホモロジーがあり，また，MYCN が増幅した神経芽腫細胞株において発現が低下していることがわかっていた。我々は，まず，神経芽腫 56 検体における BIN1 遺伝子発現を定量的 PCR にて解析した。その結果，BIN1 遺伝子発現は，神経芽腫の既知の複数の予後良好因子群において有意に高発現であり，神経芽腫細胞株における強制発現の結果，MYCN 蛋白と協調してアポトーシスを誘導することが明らかになった[8]。

また，我々は，マイクロアレイシステムを用いて新規予後関連遺伝子の検討を行った。既知の予後因子が全て予後良好である神経芽腫検体 3 検体と全て予後不良である神経芽腫検体 3 検体からそれぞれ，mRNA をプールし，cDNA マイクロアレイにて両群間の遺伝子発現差異を解析した。その結果，予後不良群に優位に発現している遺伝子群を約 400 抽出し，また，予後良好群に優位に発現している遺伝子を約 40 抽出した。その中で，胎生期の脳神経系に特異的に発現している Neuronatin（Nnat）遺伝子に注目した。Nnat は 1994 年にはじめて哺乳動物の新生児の脳からクローンされた。哺乳動物種で高度に保存されており，発生途上の哺乳類の神経系で認められる。マウスを用いた研究にて，Nnat の発現はまず胎生 8.5 日に後脳に認められ，その後，中枢神経から末梢神経へと広がっていき，出生後に徐々に消失する。交感神経系，副腎にも，マウスの胎生 15 日目に認められている。この遺伝子は 20 番染色体長腕 11.2-12 に存在しており，3973 鎖長である。3 つのエキソンと 2 つのイントロンを含み，スプライシングバリアントとして 2 つの発現型 Nnatα，β がある。α フォームは 3 つのすべてのエキソンを含み，β フォームは α フォームの中央のエキソンを除く 2 つのエキソンを含む。神経発生における Nnat の機能はまだ明らかではない。神経芽腫 70 検体にてその発現量を定量的 PCR にて測定した結果，Nnatα，β のいずれのアイソフォームにおいても，BIN 1 遺伝子と同様に既知の複数の予後良好因子群においてに高発現であり，特に Nnatβ は，既知の予後良好因子群，全てにおいて有意に高発現であった（表 1）。これらの結果から神経芽腫における新規予後関連遺伝子の可能性が示唆された[9]。Neuronatin 遺伝子の神経芽腫における機能は，まだ，不明であるが，神経芽腫細胞株（IMR32）において強制発現させると神経突起の延長が認められ，神経芽腫の成熟・分化に関与していることが予想される。

表1　70神経芽腫検体におけるNnat β発現量と予後因子

分類		Nnatβ/18s rRNA (% TILE 50%)	P value (Mann-Whitney U test)
年齢	1才未満 1才以上	1.72 0.36	$p < 0.01$
病期	stage 1,2,4S stage 3,4	1.11 0.36	$p < 0.01$
DNA ploidy	aneuploid diploid	0.96 0.33	$p < 0.05$
Shimada 分類	Favorable Unfavorable	1.79 0.14	$p < 0.01$
MYCN 増幅	なし あり	1.01 0.06	$p < 0.01$
転帰	生存 死亡	1.01 0.37	$p < 0.01$

3. 神経芽腫予後関連遺伝子解析の組み合わせによる悪性度判定システム

FISH法と定量的PCRを用いた遺伝子数的解析（MYCN増幅）と，定量的RT-PCRを用いた遺伝子発現量解析（既知予後因子のTrkA，新規予後因子のBIN1，Neuronatinβ（Nnatβ））を組み合わせることによる神経芽腫悪性度判定システムの確立を検討した。その結果，TrkA低発現，BIN1低発現，Nnatβ低発現の3予後不良因子の保有数と臨床病期及び転帰との解析の結果，3予後不良因子の保有数は神経芽腫の悪性度と有意に相関していた（図2）[10,11]。さらにこの3因子にMYCN増幅の高感度解析を加えた4予後不良因子の保有数による解析の結果，不良因子を0-4個有する症例のそれぞれの5年生存率は，0個-92%，1個-88%，2個-78%，3個-40%，4個-0%（$P < 0.001$，trend test by Kruskal-Wallis exact test）であり，この分類にて神経芽腫悪性度に関して5群の層別化が可能であった。このシステムにおけるExtremely high risk群（4不良因子）には新規治療法の開発が望まれ，Secondly high risk群（3不良因子）には，現行の強力な集学的治療法の適正な遂行，その他の群には，治療合併症を極力避けた臨床プロトコールの確立と遂行が望ましいと考えられた。

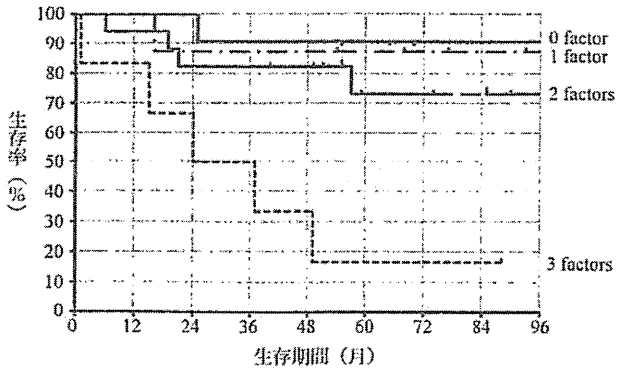

図2　3予後不良因子（TrkA低発現、BIN1低発現、Nnat β低発現）の保有数と生存率曲線

4. 難治性小児固形悪性腫瘍に対する樹状細胞を用いた免疫遺伝子治療の開発

神経芽腫は，ガングリオシドの産生，ケモカインの産生抑制，MHC class I発現抑制などによって宿主免疫より逃れていると考えられる。新規治療法の開発として我々は，樹状細胞による免疫治療に注目し，センダイウイルスベクター

(SeV) によって活性化された樹状細胞 (ts-rSeV/dF-DCs) を用いた免疫遺伝子治療を臨床応用することを目的としたマウスにおける前臨床試験を行った[12]。

A/J マウスにマウス神経芽細胞腫 C-1300 を 10^6 個皮下接種し，生着後，骨髄由来 DC を SeV にて活性化し治療に用いた。腫瘍生着後 3 日目より治療開始する群を早期治療群，10 日目より治療開始する群を後期治療群とした。ts-rSeV/dF-mIFNβ（前研究で B16 メラノーマにおいて抗腫瘍効果を効率よく増強することのできたマウス IFN-β 遺伝子を，ts-rSeV/dF を用いて樹状細胞へと導入した）を用いた場合，早期治療群では 60％の個体で腫瘍の完全消失を認め，後期治療群においても抗腫瘍効果の増強を認めた。

臨床試験に向かう前に腫瘍が十分，生着，増大した後期治療群におけるさらなる抗腫瘍効果を得るために SeV/DC 投与を行う 3 日前から，3 日間（7,8,9 日目），4Gy/day の X 線を腫瘍局所的に前照射を行う実験を行った。図 3 に示すごとく，γ 放射線単独治療，および ts-rSeV/dF-mIFNβ-DCs 単独治療のみでも効果的に腫瘍体積を減少させることはできるものの，確立された腫瘍を完全排除することは困難であった。（腫瘍の完全排除はγ放射線単独治療では 6 頭中 0 頭，ts-rSeV/dF-mIFNβ-DCs 単独治療では 8 頭中 2 頭であった）一方，この 2 つの治療を組み合わせた場合，8 頭中 6 頭において腫瘍接種後 38 日目には，確立された腫瘍の完全排除が可能となった。結果としては，γ 放射線と ts-rSeV/dF-mIFNβ-DCs を組み合わせた治療においては 8 頭中 5 頭が無腫瘍状態で 200 日を超える生存を認めた[13]。

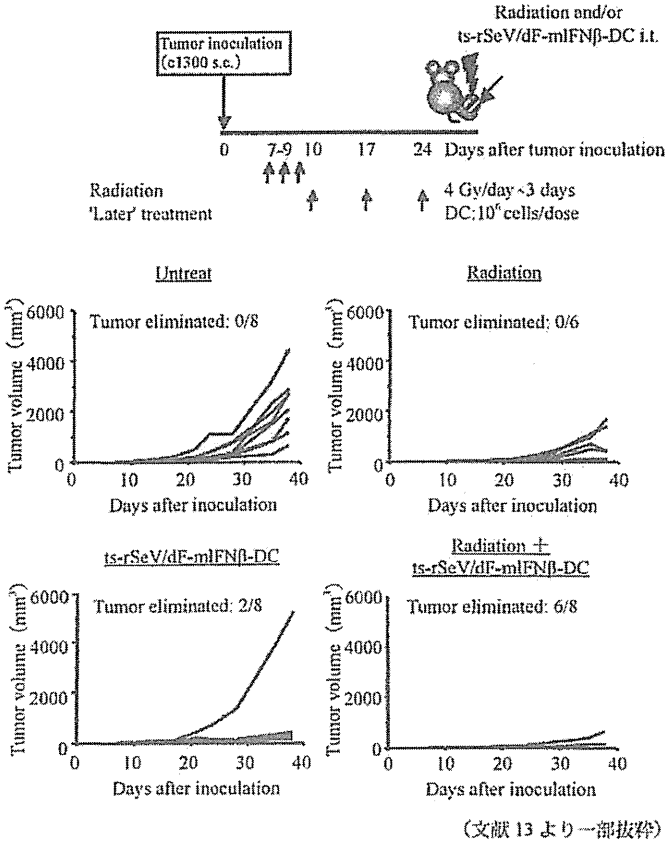

（文献 13 より一部抜粋）

図 3　放射線前照射併用 ts-rSeV/dF-mIFN β -DCs 療法の抗腫瘍効果

いずれの実験においても，抗腫瘍効果を認めたマウスにおいて腫瘍特異的な CTL の誘導を認めた。また，腫瘍接種後 186 日目に，c1300 と MuSS を同時に接種する再接種実験を行った。無治療，または臨床的に適切な放射線照射のみをした個体においては腫瘍接種後 120 日以内に全例が死亡した。ts-rSeV/dF-mIFNβ-DCs を用いた樹状細胞治療のみを行った個体 4 頭のうち，1 頭は 120 日以上，無腫瘍状態で生存したが，この個体には MuSS や c1300 の再接種により，

双方の腫瘍が生着した。放射線を過剰照射した個体4頭のうち，3頭は無腫瘍状態で120日以上生存したが，MuSS，c1300の再接種に対し，双方とも生着した。一方，γ放射線照射と樹状細胞治療との併用治療を行った個体では，4頭中3頭が無腫瘍状態で120日以上生存し，さらに4頭全てにおいてc1300の再接種を特異的に拒絶した。このことから本療法は，長期メモリーを成立させることが示唆された[13]（図4）。

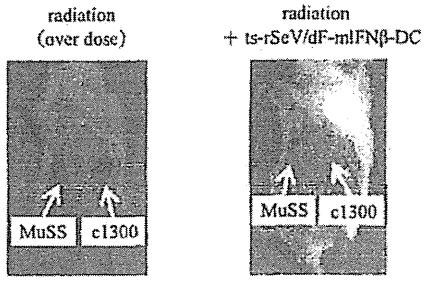

腫瘍再接種実験

	Total examined	2nd challenge (c1300 and MuSS)			
		Alive (tumor free)	used for 2nd challenge	rejection of c1300	rejection of MuSS
untreat	4	0	—	—	—
radiation (4Gy × 3)	3	0	—	—	—
radiation (over dose：34 Gy × 3)	4	3	3	0	0
ts-rSeV/dF-mIFNβ-DC	4	1	1	0	0
radiation (4 Gy × 3) + ts-rSeV/dF-mIFNβ-DC	4	3	3	3	0

（文献13より一部抜粋）

図4　放射線前照射併用ts-rSeV/dF-mIFNβ-DCs療法による永続的な腫瘍特異的防御免疫の誘導

今後，臨床応用を考えた際にさらにSeVの安全性が問題となってくるが，SeVは細胞質内において，遺伝子発現，蛋白合成を行うため宿主染色体への影響はなく，またヒトへの病原性は報告されていないため安全性は高いと考えられる。現在，外科療法に併用した臨床試験のプロトコールを作成中であり，早期の臨床応用を目指していきたい。

おわりに

小児がんは，最近の集学的治療の進歩により，飛躍的に治療成績が向上したが，今後は，さらに患者毎の20年後のQOLを重視した治療が期待され，腫瘍毎の予後関連遺伝子発現やゲノム異常の詳細な解析による悪性度診断がさらに必要になってくる。また，難治性や再発した小児がんに対しては，新規治療法の開発も必要である。今後も，このような小児悪性腫瘍に対するトランスレーショナルリサーチに積極的に取り組んでいくことが，小児がん全体のQOLを考慮した治療成績の向上につながる近道と考える。

共同研究者

宗崎良太，東　真弓，田中　桜，竜田恭介，孝橋賢一，木下義晶，田中真司，田口智章（九州大学大学院医学研究院小児外科），米満吉和（九州大学大学院薬学研究院革新的バイオ医薬創成学），文野誠久，木村幸積（京都府立医科大学大学院医学研究科小児外科学）

文　　献

1) Brodeur GM, Seeger RC, Schwab M. Amplification of N-myc in untreated human neuroblastoma correlates with advanced disease stage. Science 1984;224:1121-1124.

2) Kaneko M, Nishihira H, Mugishima H. Stratification of treatment of stage 4 neuroblastoma patients based on N-myc amplification status. Med Pediatr Oncol 1998;31:1-7.

3) Raggi CC, Bagnoni ML, Tonini GP. Real-time quantitative PCR for the measurement of *MYCN* amplification in human neuroblastoma with the TaqMan detection system. Clin Chem 1999;45:1918-1924.

4) Tajiri T, Shono K, Fujii Y, Noguchi S, Kinoshita Y, Tsuneyoshi M, Suita S. Highly sensitive analysis for N-myc amplification in neuroblastoma based on fluorescence in situ hybridization. J Pediatr Surg 1999;34: 1615-1619.

5) Tajiri T, Tanaka S, Shono K, Kinoshita Y, Fujii Y, Suita S, Ihara K, Hara T. Quick quantitative analysis of gene dosages associated with prognosis in neuroblastoma. Cancer Lett. 2001;166: 89-94.

6) Tajiri T, Shono K, Tanaka S, Suita S. Evaluation of genetic heterogeneity in neuroblastoma. Surgery 2002;131: 283-287.

7) Tanaka S, Tajiri T, Noguchi S, Shono K, Ihara K, Hara T, Suita S. Clinical significance of a highly sensitive analysis for gene dosage and the expression level of MYCN in neuroblastoma. J Pediatr Surg 2004;39: 63-68.

8) Tajiri T, Liu X, Tanaka S, Suita S, Hogarty DM. Expression of a MYCN-interacting isoform of the tumor suppressor BIN1 is reduced in neuroblastomas with unfavorable biological features. Clin Cancer Res 2003;9:3345-3355.

9) Higashi M, Tajiri T, Kinoshita Y, Tatsuta K, Souzaki R, Maehara Y, Suita S, Taguchi T. High expressions of neuronatin isoforms in favorable neuroblastoma. J Pediatr Hematol/Oncol 2007;29:551-556.

10) Tajiri T, Tanaka S, Higashi M, Kinoshita Y, Takahashi Y, Tatsuta K, Suita S. Biological diagnosis for neuroblastoma using a highly sensitive analysis of prognostic factors. J Pediatr Surg 2006;41:560-566.

11) Tajiri T, Higashi M, Souzaki R, Tatsuta K, Kinoshita Y, Taguchi T. Classification of neuroblastomas based on an analysis of the expression of genes related to the prognosis. J Pediatr Surg 2007;42:2046-2049.

12) Tatsuta K, Tanaka S, Tajiri T,Shibata S, Komaru A, Ueda Y, Inoue M, Hasegawa M, Suita S, Sueishi K, Taguchi T, Yonemitsu Y. Complete Elimination of Established Neuroblastoma by Synergistic Action of g-Irradiation and DCs Treated with rSeV expressing Interferon-b Gene. Gene Ther 2009;16:240-251.

13) 田尻達郎，田中桜，竜田恭介，宗崎良太，木下義晶，田口智章． センダイウィルス導入樹状細胞を用いた神経芽腫の免疫療法　Pharma Media　2011;No5；57-65

NR4A3, a possibile oncogenic factor for neuroblastoma associated with CpGi methylation within the third exon

SHOTA UEKUSA[1,2*], HIROYUKI KAWASHIMA[1,2*], KIMINOBU SUGITO[1], SHINSUKE YOSHIZAWA[1,2], YUI SHINOJIMA[2], JUN IGARASHI[2,3], SRIMOYEE GHOSH[4], XAOFEI WANG[2,3,5], KYOKO FUJIWARA[2,6,7], TARO IKEDA[1], TSUGUMICHI KOSHINAGA[1], MASAYOSHI SOMA[6,7] and HIROKI NAGASE[2,3,5,7]

Departments of [1]Pediatric Surgery and [2]Cancer Genetics, School of Medicine, [3]Life Science Advanced Research Institute for the Sciences and Humanities, Nihon University, Tokyo, Japan; [4]Department of Zoology, North-Eastern Hill University, Meghalaya, India; [5]Chiba Cancer Center Research Institute, Chiba; [6]Innovative Therapy Research Group, Nihon University Research Institute of Medical Science, [7]Division of General Medicine, Department of Medicine, Nihon University School of Medicine, Tokyo, Japan

Received December 18, 2013; Accepted February 12, 2014

DOI: 10.3892/ijo.2014.2340

Abstract. Aberrant methylation of *Nr4a3* exon 3 CpG island (CpGi) was initially identified during multistep mouse skin carcinogenesis. *Nr4a3* is also known as a critical gene for neuronal development. Thus, we examined the *Nr4a3* exon 3 CpGi methylation in mouse brain tissues from 15-day embryos, newborns and 12-week-old adults and found significant increase of its methylation and Nr4a3 expression during mouse brain development after birth. In addition, homologous region in human genome was frequently and aberrantly methylated in neuroblastoma specimens. A quantitative analysis of DNA methylation revealed that hypomethylation of CpG islands on *NR4A3* exon 3, but not on exon 1 was identified in three neuroblastomas compared with matched adrenal glands. Additional analysis for 20 neuroblastoma patients was performed and 8 of 20 showed hypomethylation of the CpGi on *NR4A3* exon 3. The survival rate of those 8 patients was significantly lower compared with those in patients with hypermethylation. Immunohistochemical NR4A3 expression was generally faint in neuroblastoma tissues compared with normal tissues. Moreover, the MYCN amplified NB9 cell line showed hypomethylation and low expression of *NR4A3*, while the non-MYCN amplified NB69 cell line showed hypermethylation and high expression. These results indicate that DNA hypomethylation of the CpGi at *NR4A3* exon 3 is associated with low *NR4A3* expression, and correlates with poor prognosis of neuroblastoma. Since NR4A3 upregulation associated with the hypermethylation and neuronal differentiation in mice, poor prognosis of neuroblastoma associated with NR4A3 low expression may be partly explained by dysregulation of its differentiation.

Correspondence to: Professor Hiroki Nagase, Chiba Cancer Center Research Institute, 666-2 Nitona-Cho, Chuo-Ku, Chiba 260-8717, Japan
E-mail: hnagase@chiba-cc.jp

*Contributed equally

Abbreviations: T-DMRs, tissue-specific differentially methylated regions; DS-DMRs, developmental stage differentially methylated regions; CpGi, CpG island; E15, 15-day-old embryo; NB, new born; AD, 12-week adult; TrkA, tropomyosin receptor kinase A; NGF, nerve growth factor; hMC, homogeneous MassCLEAVE; MALDI-TOF MS, matrix-assisted laser desorption/ionization time-of-flight mass spectrometry; Tm, melting temperature; PCR, polymerase chain reaction; TBS, Tris-buffered saline; PBS, phosphate-buffered saline; CTCF, CCCTC binding factor; UTR, untranslated region; AUF1, AU-rich element binding factor 1; HUR, Hu antigen R

Key words: nuclear receptor subfamily 4, group A, member 3, DNA methylation, neuroblastoma

Introduction

Neuroblastoma is an embryonic tumor of neuroectodermal cells derived from the neural crest. It is the most common extracranial solid tumor in children, and it accounts for approximately 15% of all pediatric oncology death. Survival rate of the patient with high-risk neuroblastoma is still <40%, despite combined modality therapy (1,2).

Recent advances have disclosed the significance of epigenetic events in the development and progression of human tumorigenesis. Generally, global DNA methylation levels are low in cancer and has been linked to genomic instability, which can lead to DNA damage. On the other hand, promoter-specific hypermethylation of specific genes, such as tumor suppressor genes, is the most common event in tumorigenesis (3). It is also reported that predetermined epigenetic program provides required direction for the number of changes during embryonic and postnatal development that are necessary for proceeding from an oocyte to a fully developed adult animal (4). DNA methylation is the one of the best-characterized epigenetic modifications and plays an important role in the diverse genomic processes,

Table I. The tissue samples analyzed.

Patient	Age at diagnosis (month)	INSS	INPC	Shimada classification	Copy nos. of *MYCN*	Prognosis (month)	Methylation level of *NR4A3* exon 3 (%)[a]
Case 1	6	1	NBL, D	FH	1	48S	43.1±5.9
Case 2	10	2	NBL, PD	FH	1	26S	67.1±2.5
Case 3	6	2	NBL, PD	FH	1	48S	20.1±0.9
Case 4	6	4S	NBL, UD	FH	1	48S	43.1±5.9
Case 5	6	2	NBL, PD	FH	1	48S	7.6±0.1
Case 6	7	2	NBL, PD	FH	1	48S	18.4±1.6
Case 7	8	2	NBL, PD	FH	1	48S	83.2±0.4
Case 8	26	4	NBL, PD	UH	10	6R	36.1±1.5
Case 9	36	4	NBL, UD	UH	20	48S	-0.4±8.9
Case 10	30	4	NBL, PD	UH	1	48S	34.3±2.4
Case 11	47	4	NBL, UD	UH	20	4R	8.5±1.5
Case 12	21	3	NBL, UD	UH	150	7R	2.1±7.3
Case 13	98	3	NBL, UD	UH	1	48S	-1.2±7.3
Case 14	77	4	NBL, PD	UH	3	4S	14.7±5.9
Case 15	79	4	NBL, PD	UH	3	35R	39.1±2.2
Case 16	53	4	NBL, UD	UH	4	24R	79.4±0.6
Case 17	20	4	NBL, UD	UH	81	5R	9.1±3.8
Case 18	68	4	NBL, PD	UH	1	10R	5.2±2.5
Case 19	18	4	NBL, PD	UH	119	37S	5.4±4.1
Case 20	33	4	NBL, UD	UH	1	36S	25.6±10.1

INSS, International Neuroblastoma Staging System; INPC, International Neuroblastoma Pathology Committee; NBL, neuroblastoma; PD, poorly differentiated; UD, undifferentiated; FH, favorable histology; UH, unfavorable histology; S, recurrent free survival; R, recurrent. [a]Data are shown as mean ± SD.

such as gene regulation, chromosomal stability, parental imprinting and X-inactivation (5). Recent genome-wide DNA methylation searches indicate that 4 to 17% of CpG sites are different in methylation among tissues and developmental processes (6-8). The methylation status at the tissue-specific differentially methylated regions (T-DMRs) and developmental-specific differentially methylated regions (DS-DMRs) are suggested to play important roles in development and differentiation.

Nuclear receptor subfamily 4, group A, member 3 (*Nr4a3*), also known as neuron-derived orphan receptor 1 (NOR1), is a member of NR4A subgroup of orphan nuclear receptor. In mammals, the NR4A subgroup consists of NR4A1 (Nur77), NR4A2 (Nurr1) and NR4A3 (9). The monomer form of those receptors binds to the nerve growth factor-induced clone B response element (NBRE), and homodimer or heterodimer forms bind to the Nurl response element in the promoter of their target genes which may be essential for the development of dopaminergic neurons in the midbrain (10). We identified the CpG sites in *Nr4a3* exon 3 as a mouse skin cancer T-DMR and a mouse brain DS-DMR by using analyses of restriction landmark genomic scanning (RLGS) and methyl-DNA immunoprecipitation (MeDIP), respectively (Fujiwara *et al*, unpublished data). Here, we analyzed involvement of DNA methylation at *Nr4a3* exon 3 CpGi in Nr4a3 expression, mouse brain development, neuroblastomagenesis and association with its poor prognosis.

Materials and methods

Tissue samples. C57 BL/6J mice were purchased from Jackson Laboratory (Bar Harbor, ME) and maintained in Oriental Yeast Co. Ltd (Tokyo, Japan). Brain specimens from mice at three different developmental stages: E15, 15-day-old embryo; NB, new born; and AD, 12-week adult; were disected and stored as described previously (11).

Twenty primary neuroblastoma tumors were obtained in Nihon University Hospital (Tokyo, Japan) at the time of diagnosis, from 1999 to 2007. All the analyses of those specimens were performed under the approval of Nihon University Institutional Review Boards (IRB no. 51). Neither neoadjuvant chemotherapy nor irradiation therapy was given preoperatively to any patient. Four adrenal samples were collected from a nephroblastoma patient undergoing nephrectomy and from 3 neuroblastoma patients (cases 3, 8 and 20) undergoing tumor resection. All of the samples were immediately snap-frozen in liquid nitrogen and stored at -80˚C until use. Summary of these patients is shown in Table I.

Cell lines and culture condition. Human neuroblastoma cell lines NB9 and NB69 were obtained from Riken Cell Bank (Tsukuba, Japan). Both human neuroblastoma cell lines were maintained in RPMI-1640 (Nalarai Tesque, Kyoto, Japan) supplemented with 15% fetal bovine serum (Nichirei Biosciences, Tokyo, Japan), 100 IU/ml penicillin (Gibco™,

Table II. The primers for quantitative DNA methylation analysis.

Primer name		Sequence
NR3A3-a	Forward	GGAAATTGTTAAGTGTTTTTTTATAT
	Reverse 1	CAACCACCACTTCCTAAAT
	Reverse 2	CGACCACCACTTCCTAAAT
NR3A3-b	Forward	AGTTTTAGAATTTATGTAAGAGGAAAG
	Reverse 1	CACCCAACTATCAAACTC
	Reverse 2	CGCCCAACTATCAAACTC
NR3A3-c	Forward	GAGGTGTTGTTTAGTATTTTTATGTATTTTAAGTAG
	Reverse	CTCACCTTAAAAAAACCCTTACAACC

Each reverse primer has a T7-promotor tag (5'-cagtaatacgactcactatagggagaaggct-3') for *in vitro* transcription and the forward primer is tagged with a 10 mer tag (5'-aggaagagag-3') to balance Tm.

Carlsbad, CA) and 100 µl/ml streptomycin (Gibco). The cells were cultured in a 37˚C humidified atmosphere containing 5% CO_2 maintained in appropriate conditions recommended by the manufacturers.

DNA preparation and bisulfite treatment. Total genomic DNA was extracted from mouse brains, primary tumors, neuroblastoma cell lines and normal adrenal medullas with DNeasy Tissue Kit (Qiagen, Valencia, CA) and modified by sodium bisulfite using the EZ DNA Methylation Kit (Zymo Research, Orange, CA), by following the manufacturer's instructions.

Quantitative analysis of DNA methylation using base-specific cleavage and matrix-assisted laser desorption/ionization time-of-flight mass spectrometry (MALDI-TOF MS). Sequenom MassARRAY quantitative methylation analysis (12) using the MassARRAY Compact System (www.sequenom.com) was employed for the quantitative DNA methylation analysis at CpG dinucleotides. This system utilizes mass spectrometry (MS) for the detection and quantitative analysis of DNA methylation using homogeneous MassCLEAVE (hMC) base-specific cleavage and matrix-assisted laser desorption/ionization time-of-flight (MALDI-TOF) MS (13). The MethPrimer program (http://www.urogene.org/methprimer/index1.html) (12) was used to design bisulfite PCR primers (Table II). Each reverse primer has a T7-promotor tag for *in vitro* transcription (5'-cagtaatacgactcactatagggagaaggct-3'), and the forward primer is tagged with a 10 mer to balance melting temperature (TM) (5'-aggaagagag-3'). All primers were purchased from Operon (Tokyo, Japan). Polymerase chain reaction (PCR) amplification was performed using HotStarTaq Polymerase (Qiagen) in a 5 µl reaction volume using PCR primers at a 200 nM final concentration, and bisulfate treated DNA (~20 ng/ml). After the treatment of shrimp alkaline phosphatase, 2 µl of the PCR products was used as a template for *in vitro* transcription and RNase A Cleavage for the T-reverse reaction (3' to either rUTP or rCTP), as described in the manufacturer's instructions (Sequenom hMC, Sequenom, San Diego, CA). The samples were desalted and spotted on a 384-pad SpectroCHIP (Sequenom) using a MassARRAY nanodispenser (Samsung Seoul, Korea), followed by spectral acquisition on a MassARRAY Analyzer Compact MALDI-TOF MS (Sequenom). The resultant methylation calls were analyzed by EpiTYPER software v1.0 (Sequenom) to generate quantitative measurements for each CpG site or an aggregate of multiple CpG sites. Since maldi-TOF mass methylated peaks do not denote a particular CpG site, but rather corresponds to the number of CpG sites methylated within the cleavage fragment, we decided to present average percent methylation of all CpG sites in the bisulfite PCR fragment with the standard curve.

Standard curve of DNA methylation level was made by using 0, 25, 50, 75 and 100% methylated samples. BAC DNA (RPMI-11 341L6) obtained from Roswell Park Cancer Institute (Buffalo, NY) was used as 0% methylation and M.Sss-1 double treated BAC DNA was used as 100% methylation. The PCR was carried out with a final volume of 50 µl, containing 1.0 µl of each 10.0 µM primer (final concentration 0.2 µM), 8.0 µl of 2.5 mM dNTP, 25 µl of 2 times GC Buffer (Takara Bio, Shiga, Japan), 0.5 U of LA taq (Takara Bio) and 1 µl of genomic DNA as a template. Amplification was carried out with an initial denaturing at 94˚C for 1 min followed by 45 cycles of denaturing at 94˚C for 30 sec, annealing for 1 min at the annealing temperature of each primer (60˚C), extension for 3 min at 72˚C, and then a final extension for 5 min at 72˚C. The methylation reactions were carried out in 1X M.SssI buffer with 160 µM SAM (New England Biolabs, Ipswich, MA). In total reaction volume of 50 µl, 500 ng PCR product was treated with 4U M.SssI for 1 h at 37˚C. Reactions were stopped for 20 min at 65˚C and PCR product was purified Qiagen PCR purification kit (Qiagen). This CpG methyltransferase reaction was performed twice. Then M.SssI treated PCR product was produced (14). Curve was fitted and methylation levels were modified.

Western blot analysis. All of samples were collected and total cell lysates were prepared in M-PER mammalian protein extraction reagent (Thermo, Rockford, IL) containing a protease-inhibitor cocktail (Nalarai Tesque). Proteins (20 µg) were loaded on NuPAGE + 10% Bis-Tris gels (Invitrogen Life Technologies, Carlsbad, CA) for electrophoresis. The proteins were separated at 100 mA for 1 h, then transferred to polyvinylidene difluoride membranes by using iblot transfer

for 7 min (Invitrogen). The membranes were incubated with Tris-buffered saline (TBS), containing 5% non-fat milk, 0.2% Tween-20 and a rabbit anti-NR4A3 polyclonal antibody (1:100) overnight (SC-30154, Santa Cruz Biotechnology, Santa Cruz, CA). The membranes were washed three times with a TBS containing 0.2% Tween-20. The immunocomplexed proteins were identified by reaction with a peroxidase-linked goat antibody to rabbit IgG (GE Healthcare, Little Chalfont, UK). Then these immunocomplexed proteins were detected by enhanced chemiluminescent reaction (Amersham Bioscience Inc., Piscataway, NJ). Immunoblotting with antibody to actin (Abcam, Cambridge, MA) provided an internal control for equal protein loading. Chemiluminescent detection was performed by LAS4000 (Fujifilm, Tokyo, Japan).

Immunohistochemical staining. Formalin-fixed, paraffin-embedded serial sections (4 μm) were deparaffinized in xylene, rehydrated through graded alcohols, and immersed for 15 min in phosphate-buffered saline (PBS). The sections were soaked in 10 mmol/l of sodium citrate buffer (pH 6.9) and treated in a microwave for 15 min for antigen retrieval. After antigen retrieval the endogenous peroxidase activity was blocked with 3% hydrogen peroxidase in methanol for 30 min, and non-specific staining was then blocked by 1-h incubation with normal goat serum (Nichirei Biosciences). The sections were then incubated overnight at 4˚C with 2 μg/ml of a rabbit anti-NR4A3 polyclonal antibody (SC-30154: Santa Cruz Biotechnology). The sections were treated for 30 min at room temperature with goat secondary antibody against rabbit immunoglobulins (Nichirei Biosciences). The sections were stained at room temperature for 25 min with AEC substrate kit (Vector Laboratories, Burlingame, CA). After staining with AEC substrate kit the sections were counterstained with hematoxylin.

Chromatin immunoprecipitation assays. Chromatin immunoprecipitation assays were performed essentially as previously described (15-17) with the following minor modifications. Neuroblastoma cell lines (NB9 and NB69) were fixed in 0.33 M (1%) formaldehyde for 10 min, before adding 4 volumes of ice-cold PBS containing 0.125 M glycine, to give an approximately 2-fold molar excess of glycine over formaldehyde. Then cells were washed with cold PBS containing Protease K (Nalarai Tesque). Crude cell lysates were sonicated to generate 200-1,000 bp DNA fragments. Chromatin was immunoprecipitated with 10 μl of rabbit antiserum raised against human CTCF (07-729; Millipore, Billerica, MA) per $1x10^7$ cells or with 2 μg normal rabbit immunoglobulin G (IgG; Millipore) used as a control, according to manufacturer's protocols (Millipore). PCR amplification was performed using AccuPrime (Invitrogen) in a 25 μl reaction volume using PCR primers at 200 nM final concentration and 5 μl immunoprecipitated DNA as a template. Amplification was carried out with an initial denaturing at 94˚C for 1 min followed by 38 cycles of denaturing at 94˚C for 30 sec, annealing for 30 sec at the annealing temperature of each primer, extension for 1 min at 68˚C, and then a final extension for 5 min at 72˚C, using specific primers as follows: for *NR4A3* exon 3, 5'-CTTCCCGCTCTTCCACTTC-3'; and 5'-TCACCTTGAAAAAGCCCTTG-3', Tm 58˚C; for cMYC, 5'-GTTTTAAGGAACCGCCTGTCCTTC-3' and 5'-GGA TTGCAAATTACTCCTGCCTCC-3', Tm 62˚C (18). All primers were purchased from Operon.

Statistical analysis. The Mann-Whitney U test was used to evaluate the statistical significance of the difference in the methylation level of *NR4A3* among the samples. The methylation levels were categorized by Youden index using 17 patients passed the observation period (19). The cutoff point between high and low levels of DNA methylation at each DMR was calculated by ROC curve analysis. Survival curves were calculated according to Kaplan-Meier analysis and compared with a log-rank test. Event-free survival was calculated as the time from diagnosis to event or last examination if the patient had no event. Recurrence, progression of disease and death from disease were counted as events. Death resulting from therapy complications or from second malignancy was not counted as an event but censored for event-free survival. The data were analyzed by the SPSS (Chicago, IL) for Windows. Differences were considered significant at $p<0.05$.

Results

Methylation levels at CpG sites of Nr4a3 exon 3 CpGi and its expression in mouse brain specimens. Methylation levels of each CpG site at the *Nr4a3* exon 3 CpG island in mouse brains were analyzed at three different developmental stages. This CpGi (mouse chr4:48072571-48072905 in the USCS database, February, 2006 assembly) showed higher methylation level in the brain specimens of 12-weeks-old mice (AD brain), compared with brain specimens from 15-days-old embryos (E15) or new-born mice (NB) in the analysis using Mass ARRAY EpiTYPER (Fig. 1A). The average methylation level of all CpG sites in this region was significantly higher in AD brain than in E15 and NB brain specimens (Fig. 1B). Western blot analysis revealed higher expression level of NR4A3 protein in AD brain specimens, compared with the other developmental stages (Fig. 1C).

Search for the most different somatic change within homologous Nr4a3 exon 3 CpGi in human neuroblastoma. We analyzed methylation level of human homologous region (chr4:48072371-48072905, in USCS genome database, March, 2006, NCBI36/hg18) in the surgical resected NB specimens and found that all 3 NB specimens showed significantly lower methylation level at *NR4A3* exon 3 CpGi compare to those from the matched adrenal tissues (Fig. 2). The CpGi located between *NR4A3* promoter and intron 1 was not methylated at all in either neuroblastoma or adrenal samples.

Aberrant methylation at NR4A3 exon 3 CpGi confirmed by using Mass ARRAY EpiTYPER method in additional 17 neuroblastoma specimens. Additional 17 neuroblastoma samples and 1 adrenal sample were used to confirm aberrant methylation at *NR4A3* exon 3 CpGi. Adding a new adrenal sample, all the 4 adrenal samples were hypermethylated at *NR4A3* exon 3 CpGi. The average methylation level in 4 adrenal samples was 64.6±2.1%. The methylation level of neuroblastoma specimens varied from *83.3±.. to *-0.5±0.9%, and the average value of the all samples was 27.0±25.8%, which was significantly lower than the average methylation level of 4 normal samples

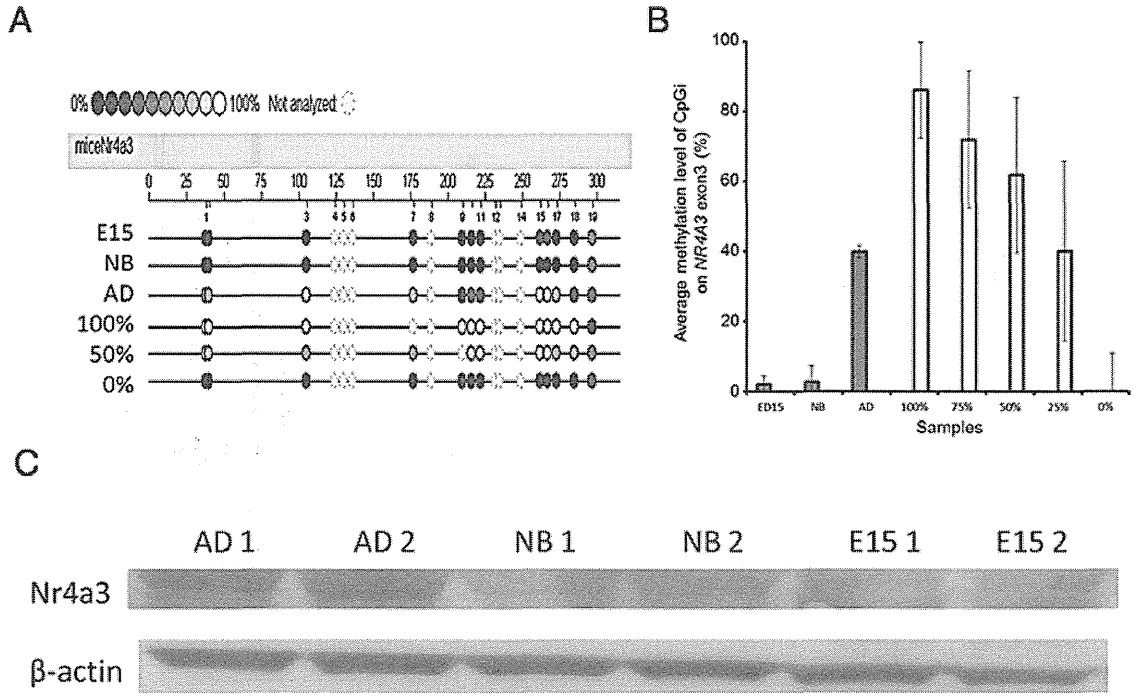

Figure 1. DNA methylation and protein expression levels of NR4A3 in mouse brain samples. DNA methylation level was analyzed quantitatively using Sequenom MassARRAY EpiTYPER. Methylation level is shown in Epigram (A) and average methylation levels are shown in the bar graph (B). Gray columns indicate mouse brain samples and open columns are the standard. Error bars indicate SD. Methylation levels in AD mouse brain samples were significantly higher than those in NB and E15 brains. ($p<0.030$). (C) NR4A3 and loading control of β-actin protein expression was analyzed by western blotting. AD brain showed higher expression level of NR4A3 than in NB and E15.

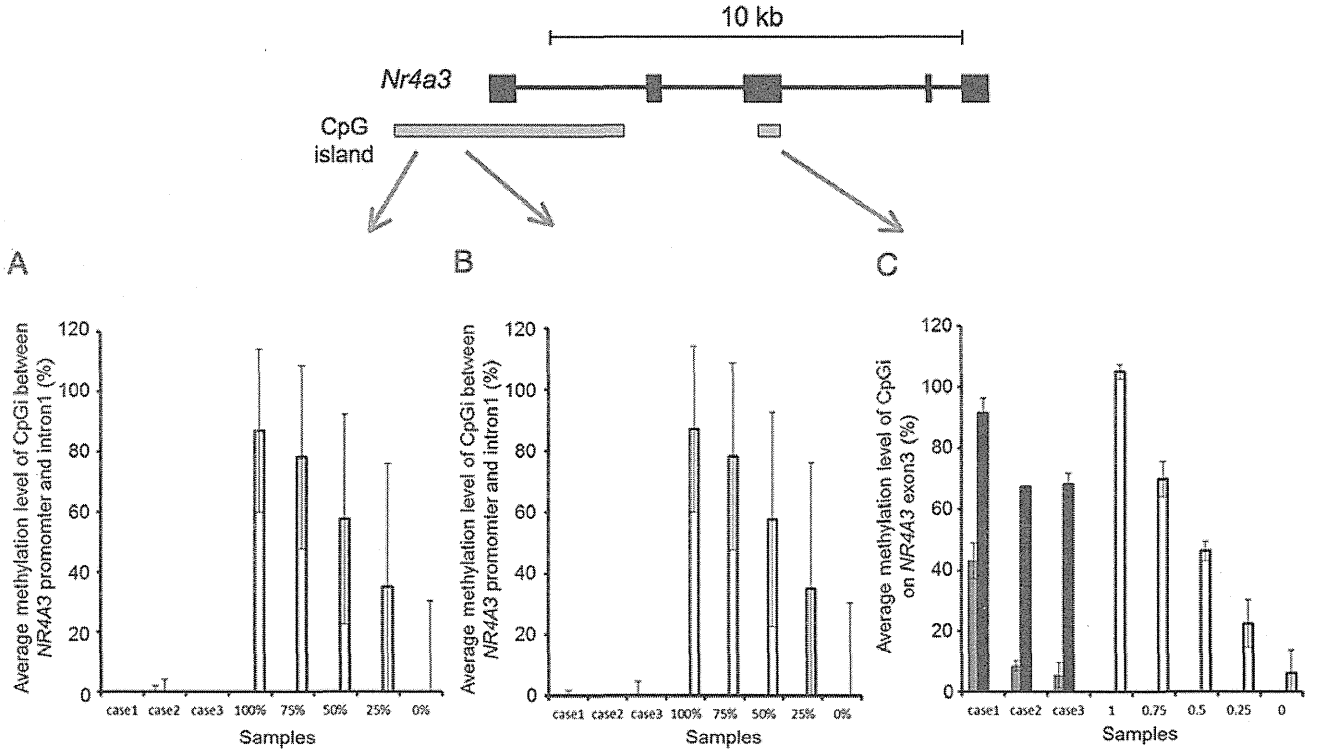

Figure 2. DNA methylation levels of the *NR4A3* region in human neuroblastoma specimens. Methylation levels of human homologous region of *Nr4a3* were analyzed quantitatively using Sequenom MassARRAY EpiTYPER in human neuroblastoma. Methylation levels of CpGi at NR4A3 exon 3 (C), but not in 5' promoter CpGi (A and B), were significantly higher in neuroblastoma than those in corresponding adrenal glands ($p<0.01$). Gray columns indicate neuroblastoma samples, black columns are for adrenal samples and open columns are the standard. Data are shown as mean ± SD.

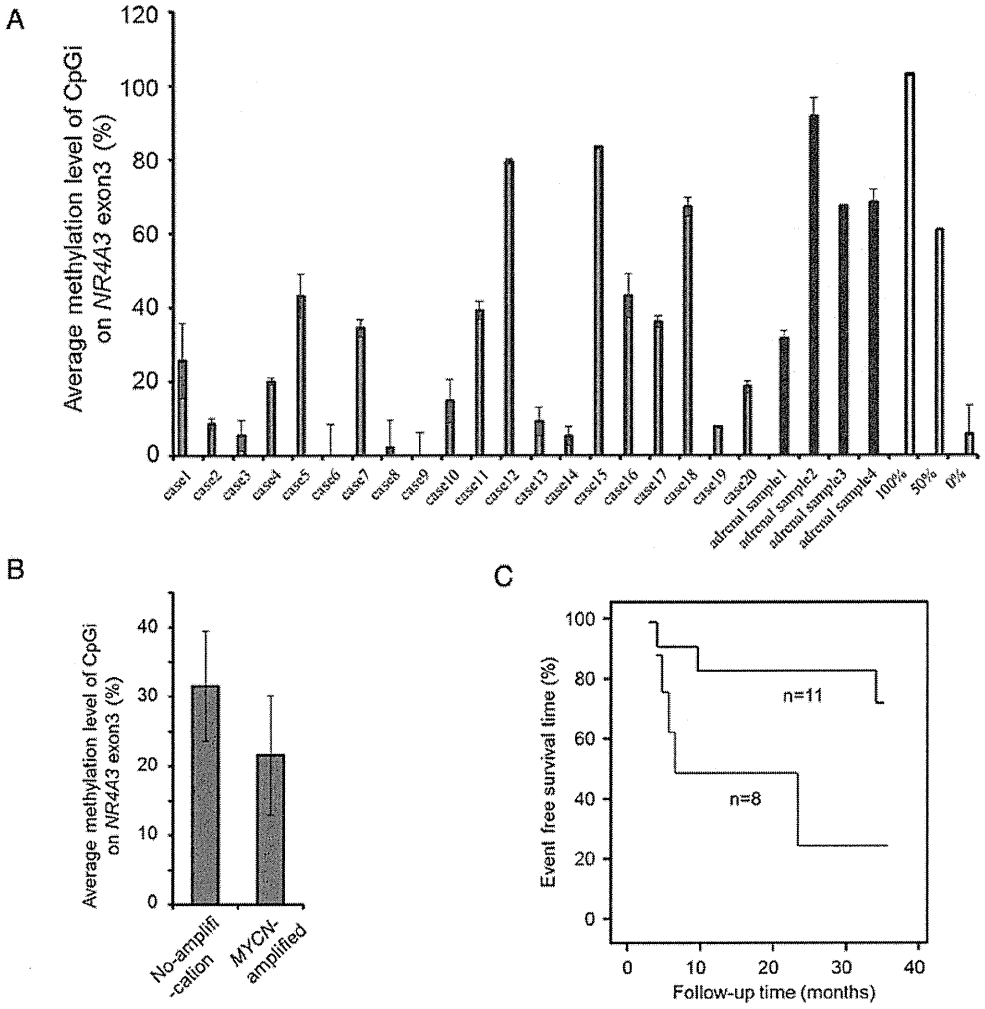

Figure 3. DNA methylation levels of *NR4A3* exon 3 CpGi in additional human neuroblastoma specimens and survival analyses of neuroblastoma patients. Methylation levels in *NR4A3* exon 3 CpGi were analyzed by using Mass ARRAY EpiTYPER method in 20 neuroblastoma specimens and 4 adrenal samples. (A) The bar graphs show the average of methylation levels in the region. Gray columns indicate neuroblastoma samples, black columns are for adrenal samples and open columns are the standard. The error bars indicate SD. (B) Average methylation level of CpGi at NR4A3 exon 3 in 11 samples without MYCN amplification and 9 samples with MCYN amplification are shown. The error bar indicate SEM. (C) Kaplan-Meier analysis was performed to see whether methylation level at NR4A3 exon 3 CpGi associate with the survival length of neuroblastoma patients. Twenty neuroblastoma specimens were segregated into two groups depending on their methylation levels of the *NR4A3* exon 3 regions (hypermethylation, methylation level is higher than 11.93%; hypomethylation, methylation level is 11.93% or lower). Eight out of 20 neuroblastoma specimens were in the hypomethylation tumor group. Black line indicates the hypermethylation group and gray line is for the hypomethylation group. There was a significant association between methylation levels and patient outcome (p=0.034, log-rank test).

(p=0.005, Mann-Whitney U test) (Table I, Fig. 3A). In 17 out of 20 neuroblastoma specimens, methylation levels at *NR4A3* exon 3 CpGi were low, compared with the average methylation level in 4 adrenal samples. Methylation level in 9 *MYCN* amplified neuroblastoma specimens was significantly lower, compared with that in 11 specimens without *MYCN* amplification (Fig. 3B) (p=0.005, Mann-Whitney U test).

For Kaplan-Meier analysis, cut off value of the methylation level was calculated as 11.93% by using youden index and the methylation levels of 20 patients passed the observation period. Twenty neuroblastoma patients were divided into two groups depending on their methylation levels at the *NR4A3* exon 3 regions. The hypermethylation group has methylation level higher than the cut off value, and the hypomethylation group showed lower than that. Eight out of 20 neuroblastoma specimens were classified to hypomethylation group. There was significant association between the methylation level at NR4A3 exon 3 CpGi and patient outcome (p=0.034, log-rank test) (Fig. 3C).

Immunohistochemical staining (IHC). Immunohistochemical analysis using NR4A3 antibody showed a strong signal in adrenal tissue sections and pronounced cytoplasmic staining. On the other hand, faint staining was seen in neuroblastoma specimens (Fig. 4).

Correlation between NR4A3 exon 3 CpGi methylation and NR4A3 protein expression in neuroblastoma cells. The average methylation level at *NR4A3* exon 3 CpGi in NB9 cells was 44±23.2%, on the other hand, it was 97.1±5.8% in NB69

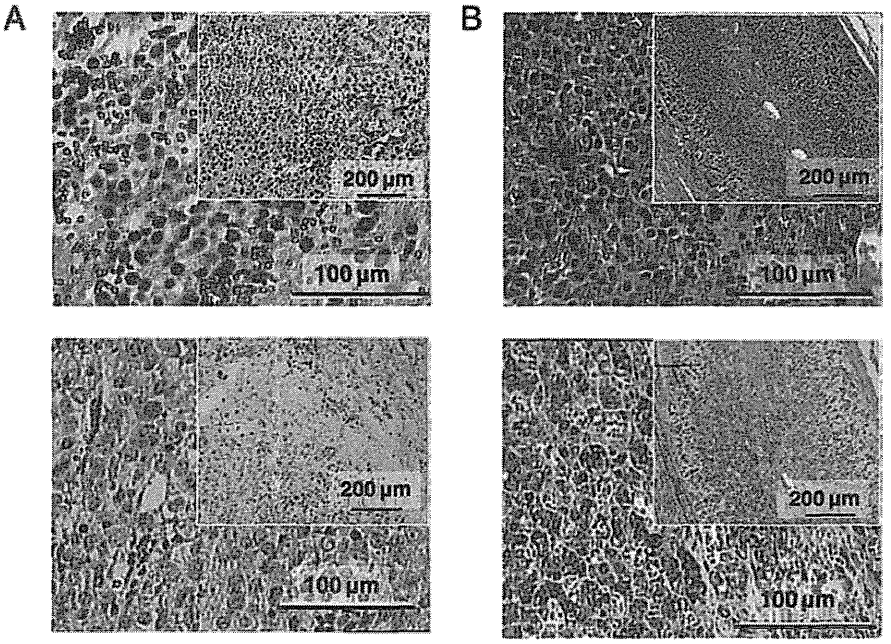

Figure 4. Imunohistochemical analyses of NR4A3 in neuroblastoma and adrenal samples. H&E staining (upper) and immunohistochemical analysis using anti-NR4A3 antibody (lower) were performed for (A) a neuroblastoma section and (B) an adrenal section. Immune reactivity was stronger in adrenal sample than in the neuroblastoma section.

cell (Fig. 5A and B). Western blot analysis revealed higher expression level of NR4A3 protein in NB69 compared with NB9 (Fig. 5C). This result also indicates that NR4A3 protein expression was correlated with *NR4A3* exon 3 CpGi methylation in human neuroblastoma cell lines.

Chromatin immunoprecipitation assays. We examined chromatin immunoprecipitation assays to elucidate the mechanism in which methylation level of NR4A3 exon 3 CpGi regulates the expression level. DNA purified from the immunoprecipitated chromatin using anti-CTCF antibody was amplified by PCR for a candidate CTCF binding site of NR4A3 exon 3. In this analysis, the amplified PCR fragment was detected clearly in NB9 cells, but not in NB69 (Fig. 5D).

Discussion

Many studies have shown that epigenetic alterations, especially aberrant DNA methylation, were involved in the development of various adult tumors (20,21). In neuroblastomas, aberrantly methylated genes, 64% for *THBS1*; 30% for *TIMP-3*; 27% for *MGMT*; 25% for *p73*; 18% for *RBI*; 14% for *DAPK*, *p14ARF*, *p16INK4a* and *CASP8*, respectively, and 0% for *TP53* and *GSTP1* have been reported and the striking differences in methylation status within neuroblastomas has suggested the existence of methylator phenotype, which might be associated with more aggressive forms of neuroblastoma (22,23). Neuroblastoma development is associated with aberration of neural differentiation, and we have reported that aberrant methylation in neuroblastoma at T-/DS-DMR, which plays an important role in differentiation and development (24).

Development of neuroblastoma is related with aberration of the function of neural development factors, such as NGF-dependent tyrosine kinase receptor TrkA activation, relating to differentiation in normal and neoplastic neuronal cells. NR4A are reported to play an important role in the development of neurons (25) and in the regulation of neural function (26). NR4A belongs to a group of early responsive genes, mediating fast response to pleiotropic extracellular stimuli. They bind to NGFI-B response element (NBRE), induce the downstream genes and affect many type of biological function such as oxidative metabolism, cell proliferation, differentiation, apoptosis and dopamine functions in the brain (9,27). In view of their role in brain function, it was reported that NR4A genes, including NR4A3, were induced by psychoactive drugs such as cocaine, morphine, haloperidol and clozapine (28). In cultured cerebellar granule neurons, NR4A transcripts translocated from nucleus to mitochondria during excitotoxicity, contributing to the induction of apoptosis (29).

Our present data about mouse brains also indicate the involvement of NR4A3 and its exon 3 CpGi methylation in the neural development. In the analysis of neuroblastoma specimens, NR4A3 exon 3 CpGi showed low methylation level in neuroblastoma compared with adrenal samples. In addition, hypermethylation of the *NR4A3* exon 3 CpGi was significantly associated with favorable outcome. Since there was a correlation between methylation level at *NR4A3* exon 3 CpGi and *NOR1* expression, our present data suggest that *NOR1* expression level and its genome methylation could be prognostic biomarkers in neuroblastoma.

Methylation of CpG sites at exonic region may be linked to epigenetic remodeling of genomic DNA structure. One of the factors is CCCTC binding factor (CTCF), which is highly conserved in higher eukaryotes. CTCF binds to CTCF-binding sites, and this binding is often regulated by DNA methylation. Of the CTCF-binding sites 45% are located on intergenic,